Your thesaurus codes are: 0.7(19.11.1;19.15.1;19.34.1:19.43.1)

The age-mass relation for chromospherically active binaries

II. Lithium depletion in dwarf components * **

D. Barrado y Navascués $^{1,2},\,$ M.J. Fernández-Figueroa $^3,\,$ R.J. García López $^4,\,$ E. De Castro $^3,\,$ and M. Cornide 3

¹ MEC/Fulbright Fellow at the Smithsonian Astrophysical Observatory, 60 Garden St, Cambridge, MA 02138, USA.

² Real Colegio Complutense at Harvard University, Trowbridge St, Cambridge, MA 02138, USA.

³ Dpto. Astrofísica. Facultad de Físicas. Universidad Complutense. E-28040 Madrid, Spain.

⁴ Instituto de Astrofísica de Canarias. E-38200 La Laguna, Tenerife, Spain.

Received date, November 25th, 1996; MArch 1997

Abstract. We present an extensive study of lithium abundances in dwarf components of chromospherically active binary stars (CABS). Since most of these binaries have known radii, masses and ages, this kind of data is especially useful for comparisons with theoretical models which try to explain the Li depletion phenomenon. We show that a significant part of these stars have clear Li overabundances with respect to the typical values for stars of the same mass and evolutionary stage. These excesses are evident when comparing our sample of CABS with binary and single stars belonging to open clusters of different ages, namely Pleiades, Hyades, NGC752, M67 and NGC188, which have ages ranging from 7×10^7 to 10^{10} yr. The Li excesses are more conspicuous for masses in the range $0.75-0.95 \text{ M}_{\odot}$, indicating that the rate of Li depletion has been less pronounced in CABS than in single stars. This phenomenon is interpreted in the context of transport of angular momentum from the orbit to the stellar rotation due to tidal effects. This angular momentum transfer would avoid the radial differential rotation and the associated turbulent mixing of material in the stellar interior. Other explanations, however, can not be ruled out. This is the case of transport of material induced by internal gravity waves, which could be inhibited due to the presence of strong magnetic fields associated with the effective dynamo in CABS. The confirmed existence of a relation between Li abundances and the fluxes in Ca II H&K lines can also be accommodated within both scenarios.

Key words: stars: activity – stars: binaries: close – stars: abundances – stars: late type

1. Introduction

The stellar group known as chromospherically active binary stars (CABS) is characterized by the presence of cool components which show emissions in CaII H&K, H α , MgII h&k, CII, CIV and other spectral lines. They have also other special characteristics, such as short orbital periods and high rotational velocities (Strassmeier et al. 1993), and include RS CVn binaries, which contain at least an evolved component, and BY Dra stars, which are still in the main sequence (MS). This last group comprises young single stars with rapid rotation and close binary stars.

This paper belongs to an ongoing project designed to study the evolution and properties of CABS. In preliminary works (Fernández–Figueroa et al. 1993; Barrado et al. 1993) we analyzed the Li abundances of a small sample, and in

Send offprint requests to: D. Barrado y Navascués, dbarrado@cfa.harvard.edu

^{*} Tables 1, 2 and 3 are also available in electronic form at the CDS via anonymous ftp to cdsarc.u-strasbg.fr (130.79.128.5) or via http://cdsweb.u-strasbg.fr/Abstract.ht ml

^{**} Based on observations collected with the 2.2m telescope of the German-Spanish Observatorio de Calar Alto (Almería, Spain), and with the 2.56m Nordic Optical Telescope in the Spanish Observatorio del Roque de Los Muchachos of the Instituto de Astrofísica de Canarias (La Palma, Spain)

Paper I of this series (Barrado et al. 1994) we described the evolutionary status of this kind of binaries, and studied a subsample of CABS having accurate mass determinations (e.g. the eclipsing binaries). Using the position of each component on a radii– T_{eff} plane, we classified a group of 50 CABS in 3 different types: MS stars having masses <1.7 M_{\odot} , evolved stars with masses around 1.4 M_{\odot} , and giants with masses in the range 2.5–5 M_{\odot} . It is also possible to discriminate 3 different evolutionary stages in the second group: subgiants evolving off the MS, subgiants at the bottom of the red giant branch (RGB), and giants ascending the RGB above the previous subgroup. Using evolutionary tracks to compute the ages of these stars, we found that the ages depend essentially on the stellar mass, and that the actual values are quite close to the corresponding ages for the terminal age main sequence (TAMS). We interpreted this relation in the context of the evolution of the internal structure and rotation, as an effect of the increase of the stellar radius as the component evolve off the MS, and the decrease of the rotation period due to tidal effects. On the other hand, since the components of CABS, (especially close binaries) do not spin down by magnetic breaking due to the transfer of angular momentum from the orbit to the stellar rotation, these stars have the needed ingredients to show an enhanced dynamo effect.

We study here a subsample of CABS with dwarf components. From now on, we will use the word dwarf to denote stars of luminosity classes V and IV which are evolving off the MS, but they have not reached the RGB. We take now into account that the abundances of light elements can change in the stellar interior as a result of different nuclear reactions. In particular, lithium is destroyed inside main sequence stars by the reaction ${}^{7}\text{Li}(p,\alpha)^{4}\text{He}$ when the temperature is higher than 2.6×10^{6} K. Late-type stars have a convective envelope which deepens with decreasing stellar mass, facilitating so the transport of material from the bottom of this well mixed zone to the Li burning layer. Because of this, Li abundances depend on mass and age for MS stars, dependence very well established by numerous studies made in open clusters and field stars (see, for a comprehensive review, Balachandran 1994). For the masses considered in this study, the actual internal stellar structure models do not predict temperatures high enough to burn Li at the bottom of the convection zone, and there should be additional mechanisms, beside pure convection, responsible of the transport of material below the convective envelope. The aim of this work is to help to discriminate between proposed theoretical mixing mechanisms. We deal here with the Li abundances of those components of CABS classified as MS stars and stars evolving off the MS, and we will present the study of Li abundances in evolved components of CABS in a forthcoming paper (Barrado y Navascués et al. 1997b, Paper III).

Following Paper I, we start by studying the evolutionary status of CABS. In this case we have used all of the data contained in the Strassmeier et al.'s (1993) catalog. We have based our discussion in the photometry of each component to classify the sample.

We describe these details and present the selected sample of dwarfs in Section 2. The observations and data reduction process are presented in Section 3. Section 4 is devoted to the measurement of Li equivalent widths (EW) and the derivation of Li abundances. Section 5 contains a comparison between CABS and single and binary stars belonging to different open clusters. The relations to other stellar parameters are shown in Section 6, and, finally, the summary and conclusions are presented in Section 7.

2. Dwarf components of CABS

2.1. The evolutionary status

In Paper I we studied the evolutionary status of CABS using a sample of binaries which have accurate values of stellar masses and radii. We concluded that CABS are in a very specific evolutionary stage, since we found a relation between their ages and the masses of the primary stars.

Our goal here is to study in detail the status of the whole sample of CABS and, in particular, to define the subsample of dwarfs components. Since an important part of the systems included in the catalog by Strassmeier et al. (1993) has no eclipses (then the radii and masses are not well known or are not known at all), the study about the evolutionary status must be conducted in a different way than in Paper I. We have used here the absolute visual magnitudes (these systems are quite near to the Sun, and most of them have measured trigonometric parallaxes) versus the (B-V) colors to produce Figure 1. We have overplotted the evolutionary tracks by Schaller et al. (1992) and Schaerer et al. (1993a) for metallicities Z=0.020 (solid lines) and Z=0.008 (dashed lines), respectively. Dwarf, subgiant and giant primaries (namely, the brightest star in the binary system) are shown as solid pentagons, squares and triangles, whereas dwarf, subgiant and giant secondaries are shown as open pentagons, squares and triangles, respectively.

In order to be able to locate most of the components of CABS in the color-magnitude diagram of Figure 1, we proceeded in different ways: for an important part of the CABS there are available values of (B-V) for each component, which were measured during eclipses. In other cases, the components have equal mass or spectral type. Then, the color should be the same and the magnitudes follow the relation $V_{\text{primary}}=V_{\text{secondary}}=V_{\text{observed}}+0.753^{\text{m}}$.

Under certain conditions (when the binary is close to the ZAMS) it is possible to perform a deconvolution process of the photometry, as described by Barrado y Navascués & Stauffer (1996), to compute individual colors and magnitudes. In a few cases, absolute magnitudes were assigned using the spectral type. Details of this process can be found in the footnotes to Table 1.

As it can be seen in Figure 1, the spectral classification does not provide clear boundaries to separate evolutionary stages of CABS. Moreover, the distinction between hot and cool components, although useful to identify the stars inside the system, is quite confusing when the evolutionary status is studied. In fact, depending on the masses of both components, the cool star can be the more massive one (and then the most evolved one in the case of a K III+F V binary) or the vice versa (the case of a K V+M V binary). Therefore, we will use the terms primary and secondary to refer the more and less massive star, respectively. When the masses are not known, the primary is defined as the most evolved star.

According to Figure 1, it is possible to classify CABS in 5 different groups:

- Stars inside the MS.
- Stars evolving off the MS or crossing the giant gap (MS-off).
- Stars at the bottom of the red giant branch.
- Those ones in the top part of the RGB.
- Components in the horizontal branch (HB).

This classification attends to differences in the physical structure of the stars and the mechanisms they use to produce energy. Then, the CABS in the second group (MS-off) have finished the hydrogen combustion in the center of the core and are expanding or developing their convective envelopes. The difference between the third and fourth groups (B-RGB and T-RGB) arises from the fact that B-RGB stars are burning helium, whereas T-RGB stars could burn also other elements. Note that this classification is in excellent agreement with that one described in Paper I based on the positions on the Radii– $T_{\rm eff}$ plane.

The age of each component of the CABS was computed using again the theoretical evolutionary tracks by Schaller et al. (1993) and Schaerer et al. (1993a,b). The method for estimating ages consists of an interpolation with radii and then, with masses, because both stellar parameters are well known for an important part of stars in our subsample of CABS containing dwarf components. As shown in Paper I, there is a clear correlation between mass and age for CABS. We have used this characteristic to assign the ages of those CABS of our sample which have known values of their masses but their radii have not been measured. The actual expression is:

$$\text{Log Age} = (9.90 \pm 0.20) - (2.84 \pm 0.06) \text{ Log (Mass/M}_{\odot}).$$

An illustration of this relation can be seen in Figure 3 of Paper I.

2.2. Program stars

The basic data –namely, photometry, stellar masses, radii, distances, orbital and rotational periods, etc– were selected from the Catalog of CABS (Strassmeier et al. 1993 and references therein). Table 1 shows the systems which have been studied in this paper: column 1 lists the name of the system, column 2 the HD number, columns 3, 4, 5 and 6 our assignation of the (U–B), (B–V), (V–R)_J and (V–I)_J colors, respectively, for each component. Column 7 lists the distance whereas the 8th, and 9th columns contain the apparent visual magnitude and the absolute magnitude computed with the previous 2 columns. In this last case, we also took into account other information in order to obtain the most accurate estimation of the magnitude of each component in the binary system (see notes in Table 1). Finally, column 10 shows our evolutionary classification (MS or MS-off star), and column 11 provides the spectral type. The last column contains notes about the method used to compute the absolute visual magnitude and the photometric indices for each component. In total, our sample has 41 systems, which contain 62 dwarf components. As far as we know, our subsample does not have any bias with respect to the whole sample of CABS.

3. Observations and data reduction

The spectra of the stars analyzed here were collected during three different observational runs. The two first ones were carried out at the coudé focus of the 2.2m telescope of the Calar Alto Spanish–German Observatory (CAHA) in June 1993 and May 1994, respectively. The last run was carried out at the Nordic Optical Telescope (NOT, 2.56m) of the Spanish Roque de Los Muchachos Observatory (La Palma) in September 1994.

For the first observational campaign we used the Boller and Chivens spectrograph equipped with a FRD CCD (1024×1024 pixels, 13μ m/pixel) at the F/3 camera and a GEC CCD (1155×768 pixels, 22.5μ m/pixel) at the F/12

(1)

camera. A slit of 1 arcsec was used, and the spectral resolution achieved (measured from the FWHM of Th–Ar emission lines spectra) was R \sim 30 000 in both cases. For the second campaign we selected the RCA CCD at the F/3 focus, (1024×1024, 15 μ m/pixel, R \sim 30 000) and the TEK CCD at the F/12 focus (1024×1024, 24 μ m/pixel, R \sim 50 000). Finally, the observations at the NOT were performed using the IACUB echelle spectrograph (McKeith et al. 1993) at the Cassegrain focus of the telescope, with a Thomson 1024 × 1024 CCD detector. A final resolution of about 40 000 was obtained.

Exposure times were estimated in order obtain signal-to-noise (S/N) ratios in the range 100-160. Since the visual magnitudes of our objects are very different $(1^m \le V \le 11^m)$, we took exposures from 5 s up to 3600 s. In order to avoid the presence of cosmic rays, several exposures were taken for the longest exposures until the required S/N ratio was achieved, adding them at the end of the reduction process. Although radial velocities are important in some cases due to the fact that the orbital periods are short, the exposure times were not long enough to produce an important doppler broadening of the lines, since in those cases the rotation is itself quite important and is by far the main source of the broadening.

We reduced the data using standard procedures (bias subtraction, flat–field correction, extraction of onedimensional spectra and continuum normalization) and the MIDAS¹ package. For the CAHA data we transformed the pixel scale into wavelength scale by comparison with Th–Ar lamp spectra. For the NOT data, we calibrated the spectra by comparison with photospheric lines of the solar spectrum taken by observing the Moon with the same instrumentation. The wavelength calibration is extremely important, since a considerable part of our binaries are double–lined systems and the theoretical positions of the Li features of both stars were computed previously to compare with the observed wavelengths.

4. Lithium abundances

4.1. Equivalent widths

The ⁷Li I 6707.8 Å feature is in fact a spectroscopic doublet separated by 0.15 Å (6707.76 and 6707.91 Å, Andersen et al. 1984). With the resolutions of our spectra, the doublet appears as a single line. Moreover, since most of our stars are rapid rotators, the Li features are blended with the Fe I 6707.4 Å line. On the other hand, 28 out of 41 systems of our sample are SB2 systems (double–lined systems), and the Li I+Fe complex can also be blended with other spectral features arising from the other component.

In order to measure the Li equivalent width (EW), we have fitted Gaussian profiles to the spectra. Phases were accounted for during this process. Using the published ephemerides (Strassmeier et al. 1993 and references therein), we computed the positions of the lines arising from each component and used this information when fitting and measuring the equivalent widths.

Different situations appeared when we were performing the fitting procedure:

- SB1 systems with vsin i≤23 kms⁻¹. The blends between LiI and FeI lines were weak and we were able to separate the Fe contribution with the fitting procedure. We used the comparison between the measured EW(FeI 6707.4 Å) with empirical values obtained from (B–V) color indices (Soderblom et al. 1990) as a quality control of the procedure. We also obtained new empirical relations between EW(FeI 6707.4 Å) and the equivalent widths of other spectral lines such as FeI 6703.6 Å & FeI 6705.1 Å and different colors.
- SB1 systems with vsini>23 kms⁻¹. We measured EW(Li+Fe) and eliminated the Fe contribution taking into account the EW of stars with the same (B–V) color, and the empirical fits described above between EW(Fe I 6707.4 Å) and the EWs of other iron lines.
- SB2 systems where we measured in the spectrum $\Delta v_r > 23 \text{ kms}^{-1}$ (where the difference of radial velocities between components is defined as $\Delta v_r = |v_r^{\text{primary}} v_r^{\text{secondary}}|$) and no blend with other close lines from the other component. The Li features from both components appeared separated. We proceeded like in the first case.
- SB2 systems with multiple blends and narrow lines. We fitted as many Gaussian curves as necessary to obtain the EW(Li).
- SB2 systems with multiple blends and wide lines. We measured the whole EW and tried to take out the different contributions with empirical relations between lines and colors.

Some examples of these fitting procedures can be found in Figure 2. On the other hand, the continuum location is very important. There are uncertainties due to blends with other lines and the noise of the spectra. As a rule, we located the continuum in the middle of the noise distribution for each wavelength.

¹ Munich Image Data Analysis System is a program developed by European Southern Observatory, Garching

Since most of our spectra have a secondary component bright enough to contribute to the continuum of the primary star, a correction of the measured EW is necessary. The continuum correction factors –CCF– were calculated using the equation:

$$CCF = \begin{cases} (1+\alpha), & \text{for hot components} \\ (1+\alpha)/\alpha, & \text{for cool components'} \end{cases}$$
(2)

where α is defined (Boesgaard & Tripicco 1986b) as:

$$\alpha = \frac{e^{(2.146 \times 10^4 / T_{eff}^{col})} - 1}{e^{(2.146 \times 10^4 / T_{eff}^{col})} - 1} \times \left(\frac{R_{cool}}{R_{hot}}\right)^2 \qquad ,$$
(3)

or, in the cases the radii (R_{hot}, R_{cool}) were not available, we used the relation between the fluxes derived from the apparent magnitude of the primary and secondary $(V_{\rm p}, V_{\rm s})$, defined as:

$$\alpha = 10^{-(V_s - V_p)/2.5}.$$
(4)

The differences between both methods are irrelevant. Then, the final EWs were obtained using:

$$EW^{corrected} = EW^{measured} \times CCF.$$
(5)

The results are shown in Table 2. In columns 1 and 2 we list the name of the star and its HD number, while columns 3 and 4 contain the parameters –effective temperature and radius– needed to compute the continuum correction factors (CCF), listed in column 8. The method to compute CCF is indicated in column 9. Columns 5, 6 and 7 provide the measured equivalent widths of Li I 6707.8 Å plus Fe I 6707.4 Å, and only the iron line or the lithium doublet, respectively. In these two last cases, the values are not corrected by the effect of the continuum due to the presence of a companion star.

4.2. Effective temperatures

We have used different photometric temperature scales to compute the final effective temperatures. Since most of our stars have available (B–V) colors, this index has been our basic temperature indicator. We estimated these temperatures with the scale provided by Thorburn et al. (1993). However, for the coolest stars in our sample, we selected scales based on (V–I)_J (Cayrel at al. 1985) and (R–I)_J (Carney 1983), and the final T_{eff} was computed as the average of these values. For some cases, photometry is not available and we have used only the spectral type to compute the effective temperature (Schmidt–Kaler 1982). The standar deviation of the differences between temperatures obtained from color indices and from the spectral types, for those stars having both, is 320 K.

We verified that this procedure does not introduce any bias in the final temperatures and abundances. In fact, we computed, when possible, the different temperatures for the stars in our sample and compared them. Except for stars having temperatures less than 4500 K, there are neither significant differences (the average value is 80 K) not any clear trend. The differences in the lower range of temperatures are easy to understand since the Thorburn et al. (1993) temperature scale was obtained using stars with higher temperatures.

4.3. Lithium abundances and errors

In order to estimate the Li abundances, we used the Pallavicini et al. (1987) curves of growth (COG), valid for $4500 \leq T_{\rm eff} \leq 6500$ K. In those cases where the effective temperature was lower, we used the COG computed by Soderblom et al. (1993). All these COG were computed under LTE conditions and a gravity value of Log g=4.5. Systematic differences between the results obtained with both sets of COG were avoided by modifying the last group following the technique described by Duncan & Jones (1983). This consists in computing the differences between the curves obtained for a given temperature (in our case, 4500 K) and shifting a whole set with these values. Then, the positions of both curves at 4500 K would overlap. The maximum value of the differences, in the linear part of the curves at any temperature, is 0.1 dex.

In addition to our data, we have included the available measurements present in the literature. Specifically, we have re–analyzed the data by Pallavicini et al. (1992), Fernández–Figueroa et al. (1993), and Randich et al. (1993) using similar procedures. The final corrected EW(Li) and abundances are listed in colums 4 and 5 of Table 3. This table also contains information about the stellar masses, orbital and photometric periods, and ages (computed by interpolating radii and masses with isochrones or from the relation between ages and masses for CABS, see Eq. 1 in Section 2).

In general, spectral synthesis provides more accurate abundances because it allows to remove different effects, such as the blends with other lines at similar wavelength. However, in the specific case of CABS, Randich et al. (1993) have shown that there are no important differences between abundances derived using COG and those obtained using synthetic spectra techniques. Other studies show similar results (eg. Barrado y Navascués et al. 1997a). Moreover, under special circumstances it is not possible to compute a reliable synthetic spectrum for some binaries because there is not accurate information. Since the goal of this paper is to study the evolution of the Li abundance in a large sample of dwarf components of CABS, it is reasonable to use COG to derive Li abundances. On the other hand, as mentioned above, the use of COG allows us to include in our analysis the EW(Li) provided in the literature.

Abundances were derived assuming LTE conditions. There are two ways in which the abundances could be affected by stellar activity *per se.* On one hand, there could be significant NLTE effects due to the presence of the chromosphere. As shown by Houdebine & Doyle (1995), the inward UV and optical flux can reheat the upper atmosphere and modify the continuum level. Therefore, the observed EW(Li) would be smaller than that of a non active star for the same abundance, metallicity and mass. This effect would be relevant when the H α line appears in emission and when the abundances are high, but none of our stars presents both characteristics simultaneously. Note that this effect is opposed to the overabundances we have found (see next subsection). Then, we consider that the excesses in the Li abundances are real, and the NLTE is a second order effect in the Li abundance determination for our stars. Moreover, Pavlenko et al. (1995) have shown that the differences between Li abundances calculated under LTE and NLTE conditions for stars with $T_{\rm eff} \leq 5500$ K are significant only for very strong lines. On the other hand, stellar spots could modify the Li abundance determinations. There are two associated effects: first, the spots can change the photometric indices and, therefore, the inferred $T_{\rm eff}$ which will be used to compute the abundances. Second, the EW(Li) is larger in spots than in the quiet photosphere, as shown by solar observations (Giampapa 1984). However, these effects will not modify the abundances more than ~0.30 dex altogether in the worst case (Barrado y Navascués 1996).

In addition to the previously described phenomenon associated with the presence of stellar spots, there are other different sources of errors in the Li abundance determinations, such as the EW measurement process, the effective temperature scale adopted, the computed continuum correction factors, and the results provided by different curves of growth. We have estimated the errors in our sample as follows: for two typical stars with 6000 and 5000 K, we have corrected EW(Li)s of \sim 50 and \sim 20 mÅ, respectively. The error in these measurements is \sim 20%. These numbers are translated into errors in the abundances equivalent to 0.16 and 0.13 dex in each case. On the other hand, the most important source of error appears in the temperature determination. The average error in the adopted effective temperatures is 200 K, and it produces uncertainties of 0.22 and 0.24 dex, respectively, in the abundances for both temperatures. The uncertainty in the continuum correction factors can be estimated in 10%, introducing additional errors of 0.06 and 0.05 dex. Finally, the errors of LTE curves of growth add another \sim 0.13 dex (Pallavicini et al. 1987). The final errors can be computed using the expression:

$$\Delta \operatorname{Log} N(\operatorname{Li})_{\operatorname{final}} = \{ \sum_{i} (\Delta \operatorname{Log} N(\operatorname{Li})_{i})^{2} \}^{1/2},$$
(6)

where $\Delta \text{Log N(Li)}_i$ are the individual errors described above. For both temperatures, the final value is 0.31 dex. If the possible presence of spots is taken into account, it would lead to a maximum error of 0.43 dex. As noted by Randich et al. (1993), although these errors can be very important for individual stars, they cancel each other and do not affect to the conclusions reached when studying the whole sample of stars.

4.4. Li abundance vs. effective temperature

As shown by Cayrel et al. (1984), Balachandran et al. (1988), García López et al. (1994), and several other works, Li abundances of stars belonging to open clusters are strongly related to the stellar mass or effective temperature. Figure 3a shows the Li abundances of our sample of dwarf components of CABS against T_{eff} –solid circles–. For comparison purposes, we have also included members of the Pleiades (70–120 Myr, Meynet 1993) and Hyades (600–800 Myr; Mermilliod 1981, Gilroy 1989) open clusters. Abundances from Pleiades were selected from Butler et al. (1987), Pilachowski & Hobbs (1987), Boesgaard et al. (1988), Soderblom et al. (1993) and García López et al. (1994), whereas those from Hyades stars were obtained from Boesgaard & Tripicco (1986a), Rebolo & Beckman (1988), Thorburn et al. (1993) and Barrado y Navascués & Stauffer (1996). Pleiades stars are plotted as open triangles, whereas Hyades stars are included as open circles. The average behavior of single members of this cluster is shown as a solid line.

A first inspection of this diagram shows that the Li abundance of CABS depends strongly on T_{eff} , as happens in open cluster stars. The estimated abundances for CABS are in some cases similar to those present in Pleiades stars. It could be concluded then that these CABS have Pleiades' age. Other CABS, having abundances smaller than the Hyades, would be older than 600–800 Myr. Moreover, it would be possible to constrain the age of the cooler stars in

our sample ($4500 \ge T_{eff} \ge 3000$) between 70 and 800 Myr. However, this interpretation does not seem to be correct, for two reasons: first, it is a well known fact that low mass CABS belong to the old disk population (Eker 1992), and, therefore, their ages are between 10^9 and 5×10^9 yr, depending on the velocity dispersion. Second, the analysis presented in Paper I shows that the ages of these systems are much older than the Hyades, at least for those stars having masses larger than 0.8 M_{\odot}.

On the other hand, the scatter in the abundances of CABS is as large as that present in Pleiades, and much larger than that corresponding to Hyades stars. The scatter observed in late-type stars of the Pleiades has been associated with the effect that rotation can have in the Li depletion phenomenon (García López et al. 1994). Young rapid rotators would inhibit the Li depletion during their premain sequence phase (PMS) due to the effect of rotation on the internal structure (Martín & Claret 1996). During the MS phase, the scatter could be due to the lack of transfer of angular momentum and material between the envelope and the core (Pinsonneault et al. 1992). It could also be very important the role of magnetic fields in the inhibition of transport of material to the stellar interior (Spruit 1987; Schatzman 1993). Part of the scatter in the abundances observed in the Log $N(Li)-T_{eff}$ plot for CABS is due to a dependence on the stellar mass. Since an important part of our sample are quite evolved objects, and in fact in several cases they are leaving the main sequence, it is possible to have several CABS of different masses at the same temperature, as it is shown in Figure 3b. We have also included in the figure the sample of nearby dwarfs studied by Favata et al. (1996), and the Li depletion isochrones by Chabover (1993; from top to bottom, for 50, 70, 300, 800 and 4500 Myr.). As noticed by Favata et al. (1996), the observed dependence of Li on the temperature is not real, it is introduced by the conversion on the EW upper limits into abundances. The comparison between these two samples of old dwarfs allows us to determine that CABS have undergone a process of inhibition of their Li depletion. This phenomenon was previously established by Randich and Pallavicini (1991) and Pallavicini et al. (1992), using a sample of CABS which contained essentially giant stars. Our study, which makes use of dwarfs and therefore allows direct comparisons with open clusters, clearly confirms and supports this result. A more extensive discussion will be carried out in Sections 5 and 6.

5. Comparison with open clusters

As noticed above, Figures 3a,b are affected by the evolution of some stellar parameters such as temperature when a star approaches or crosses over the TAMS. To avoid this and the possible consequences on the interpretation of the abundances, we have compared them against stellar masses (Figure 4). In the particular cases of CABS, these values have been computed directly in most of cases because there are available accurate orbits for both components, with uncertainties below ~0.05 M_{\odot}. For a few binaries, we estimated the masses using the M×sin³i values (obtained from the radial velocities curves) and the inclination of the orbit (from the rotational periods and vsin i), the position in color-magnitude diagrams or the radii-T_{eff} plane (see footnotes in Table 3). The masses of cluster stars were estimated from isochrone fitting, following Balachandran (1995).

Figure 4a compares the abundances against stellar masses for our sample of CABS and Hyades binaries. Note that we have differentiated tidally locked binary systems (TLBS) from well separated systems (Barrado y Navascués & Stauffer 1996). In fact, some of the Hyades TLBS have been catalogued as CABS by Strassmeier et al. (1993). Barrado y Navascués & Stauffer (1996) have studied the Li abundances of TLBS in the Hyades and concluded that they show clear overabundances when the orbital period is less than 8 days, in excellent agreement with the theoretical predictions by Zahn (1994). In our case, we have a larger sample of stars, which are older than those and have P_{orb} ranging from less than 1 day to more than one hundred.

Since CABS are, in general, older than Hyades stars, they have had more time to synchronize their orbital and rotational periods. Therefore, binaries with larger P_{orb} are TLBS. As in the Hyades, there is a relation between Li abundances and P_{orb} , in the sense that, for the same mass, (e.g. ~0.8 M_☉), Li tends to be higher in the case of TLBS than in the case of non-TLBS. Due to the fact that TLBS with $P_{orb} > 8$ d have achieved synchronization during their MS life time (Zahn 1994), the Li inhibition should have taken place, at least in part, during this stage of the evolution. In Figure 4a, CABS show some differences with Hyades binaries: First, an important part of CABS have larger abundances than Hyades stars of similar mass, despite the fact that the studied CABS –except 42 Cap– have the same age than Hyades or they are older. Second, the Li abundance scatter is much larger, and in the particular case of ~0.8 M_☉ Li abundances change by a factor 16 000. The abundance spread for a given mass in an old cluster is never larger that ~1 dex. Since CABS of equal masses have similar ages, the observed scatter should be related to other parameters. The presence of excesses in the Li abundances of at least some of our binaries at ~0.8 M_☉ can be related to the results found by García López et al. (1994) for stars with similar masses in the Pleiades. They showed that the abundances of stars having this mass are quite sensitive to rotation, and that the fast rotators deplete less Li than the slow ones.

On the other hand, it is worth to notice the detection of Li in very low mass stars, in particular YY Gem and V1396 Cyg. However, these abundances should be taken with some caveats since at these low temperatures the spectrum of late type stars presents multiple lines, together TiO and other molecular bands which were not taken into account to measure EW(Li+Fe).

It is possible to conclude from Figure 4a that the Li depletion is also less pronounced in CABS than the Hyades for those stars located in the mid F dip (Boesgaard & Tripicco 1986a), despite that the CABS are more evolved and should have started to mix the external material with material poor in Li from inside, in the so called dilution process (Iben 1965).

Figures 4b,c,d present a comparison between the abundances of CABS with members of the NGC752, M67 and NGC188 open clusters, which have ages corresponding to $1.7-2.0\times10^9$ (Hobbs & Pilachowski 1986a; Meynet et al. 1993), $3.0-6.0\times10^9$ (VandenBerg 1985; Hobbs & Pilachowski 1986b; Spite et al. 1987; García López et al. 1988; Montgomery et al. 1993; Meynet et al, 1993; Balachandran 1995; Barrado y Navascués et al. 1997c), and $6.5-10.0\times10^9$ yr (VandenBerg 1985; Meynet et al. 1993; Hobbs & Pilachowski 1986b), respectively. In these figures, open cluster stars are whown as open symbols, CABS having similar ages to the clusters appear as solid squares, and other CABS are overplotted as solid circles. These figures show, as in Figure 3, that the Li abundance scatter could be attributed to an age spread. However, we have shown in Paper I that dwarf CABS are near the TAMS, and therefore they are much older, in most of cases, than these clusters.

It is very interesting to perform a comparison using different mass intervals. Except the CABS belonging to the Hyades, which are outside of the validity of the mass-age relationship for CABS due to their low mass (the relation was computed for stars having masses larger than 0.8 M_{\odot}), all CABS classified as MS are older than NGC752 (see Figure 4b). Only some CABS located in Figure 1 above the MS (MS-off) have ages comparable to this cluster. These stars have masses in the range of the mid F dip, and should have severely depleted their Li due to one of the mechanisms that work in that region (see Balachandran 1995 and references therein) and also should have started to dilute its abundance due to the mixing of material as the star develops a deep convective envelope.

On the other hand, the comparison of masses ~1.4-1.2 M_{\odot} , corresponding to the cool side of the Li dip, in Figure 4c, between the CABS and M67 shows some clues about the Li depletion phenomenon when binaries start to evolve off the MS. In this figure, binaries and single stars of M67 are represented as open triangles and squares, respectively. As it can be seen, there is not a clear correlation between binarity and Li abundances in M67, despite the fact that in average they have higher abundances than single stars. A more detailed study about the Li abundances in binaries of M67 can be found in Barrado y Navascués et al. (1997c). In this mass range, which contains few CABS, only one shows a clear overabundance. Therefore, it seems that Li depletion is not affected in a large extent for this mass range. However, the Li excesses are more conspicuous in the case of CABS having smaller masses, since they are older than M67. They present the Li doublet in their spectra, so it is possible to derive abundances, when most of the M67 stars have only upper limits due to the lack of this feature in their spectrum. Finally, Figure 4d contains data of the oldest open cluster considered: NGC188. The conclusion is the same one as above, dwarf CABS have abundances larger than the values corresponding to their age. These results agree with the study by Spite et al. (1994). They found that close binaries belonging to the old disk population or the galactic halo have systematically larger abundances than binaries with larger orbital periods or single stars. Other excesses for the abundances of dwarf binaries have been found by Ryan & Deliyannis (1995).

Another way to demonstrate the excesses in the Li abundances of CABS is shown in Figure 5. Here, the ages are plotted against the average Li abundances for some mass ranges. Symbol sizes increase with stellar mass (see key). Error bars (0.17 dex for the age) are also shown. We also have included the average abundances for different ages, computed from cluster stars in three mass ranges ($0.85 \text{ M}_{\odot} \leq \text{Mass} < 0.95 \text{ M}_{\odot}, 0.95 \text{ M}_{\odot} \leq \text{Mass} < 1.05 \text{ M}_{\odot}, 1.05 \text{ M}_{\odot} \leq \text{Mass} < 1.15 \text{ M}_{\odot}$). These average values were obtained using Li abundances derived in single stars which belong to open clusters, such as Pleiades, UMa Group, Coma, Hyades, NGC 752, M67 and NGC 188. We have carried out several fits of the type Log N(Li) = A + B Log Age, one for each mass interval. Despite their age, CABS have high Li abundances. In some cases much higher than those ones characteristic of single stars at the same age. The difference becomes extreme when the comparison is made considering stars with M < 0.95 M_{\odot}, corresponding to the two smaller circle sizes and the two bottom fits. Then, we conclude that the Li depletion rate is completely different, and slower, in CABS that in single stars.

6. Li abundance, stellar activity and rotation

One possible explanation for the high Li abundances present on the surfaces of CABS is the creation of Li via spallation reactions during very active episodes, in particular flares. In fact, Pallavicini et al. (1992) and Randich et al. (1993) tried to use this hypothesis to explain the overabundances that they found in their samples of CABS, essentially

composed by giant stars. Several checks of this hypothesis have been carried out, since the creation of Li would imply a specific ratio between the isotopes 6 Li and 7 Li. Also, energetic criteria seem to reject the possibility of creation of Li at large scale. However, ⁶Li has been detected in HD84937 (Smith et al. 1993, Hobbs & Thorburn 1994), an F-type metal-poor dwarf, and the calculations performed for Population II stars by Deliyannis & Malaney (1995) indicate that it is possible to create Li in enough amount during the flares to substitute the depleted material, but, in principle, this mechanism is restricted to dwarfs and subgiants which have very shallow convective envelopes. The creation of Li during flares should produce a relation between the Li abundances and some activity indicators such as $H\alpha$, CaII H&K, the Call infrared triplet, MgII h&k, etc. We have tried to find out if there are such relations for our sample of CABS. From the available data in the literature, we have found no obvious relation between the X-ray luminosity (Dempsey et al. 1993), or H α (Montes et al. 1996). The lack of relations would indicate that there is no relevant Li creation during flares. However, there is a relation between Li abundances and the surface fluxes in CaII H&K, as provided by Fernández–Figueroa et al. (1994) and Montes et al. (1995). This relation only shows up when specific ranges of masses are selected. In Figure 6 we have plotted the Li abundances against Ca II H&K fluxes for stars having masses lower than 1.25 M_{\odot} and masses in the range $3.0 \le M \le 5.0$ M_{\odot}. (We have included data corresponding to giant components of CABS in this figure, see Paper III.) An obvious interpretation of this phenomenon would be that the presence of stellar spots, due to the high activity rates, could modify the measured Li equivalent widths, since the Li I 6707.8 Å feature is very sensitive to variations in the temperature (almost all Li is ionized in the considered range of temperature). Therefore, a stellar surface covered in a large proportion by spots would have a Li equivalent width larger than that one corresponding to the quiet photosphere, for a given value of the abundance. If this effect would not be corrected, the computed abundance would be larger than the real value.

Several works have tried to estimate the importance of this effect. Soderblom et al. (1993) performed different calculations to see if the observed spread in the Log N(Li)-T_{eff} plane for the Pleiades cluster could be attributed to this situation. They obtained that only an extreme situation (when the fraction of the surface covered by spots –filling factor– were very high) could account for the spread. Moreover, Barrado y Navascués (1996), using solar observations of the Li I 6707.8, K I 7699 and Na I 5896 Å lines in different solar regions, computed a grid of simulations under different conditions (spots of different temperatures, presence of plages, different filling factors for the spots and the plages). He found that normal situations for CABS (filling factor up to 0.30) could only introduce maximum errors smaller than 0.30 dex in the Li abundances. A different strategy was adopted by Pallavicini et al. (1993). They studied carefully four active stars, trying to find correlations between the photometric variability and changes in the shape and the equivalent widths of the Li feature. They found no proves of changes in the Li related to surface inhomogeneities.

All these evidences, together with the fact that we have not measured abundances larger than the so called "cosmic abundance", which corresponds to the abundance observed in young objects which have not undergone any depletion process (Log N(Li)=3.2, Martín et al. 1994), allow us to conclude that, with some caveats, there is no significant creation of Li, if any at all, on the atmosphere of CABS, and that the surface inhomogeneities do not affect essentially the computed abundances.

Our interpretation of the relation between Li abundances and Ca II H&K fluxes goes in other direction: the synchronization between the rotational and the orbital periods. This peculiarity would affect the transport mechanism in the stellar interior, inhibiting the depletion of Li. Figure 4a shows that TLBS have, in average, larger abundances than other CABS without coupling between the orbital and rotational periods. The stars undergoing a magnetic breaking by stellar winds would transfer angular momentum from the convective envelope to the radiative core to avoid intense radial differential rotations, and this angular momentum transfer is accompanied by mixing of material in the stellar interior (Pinsonneault et al. 1989, 1990, 1992; Chaboyer et al. 1995). If magnetic breaking is inhibited in TLBS, similar stars in different systems deplete Li in a different amount, because they have different orbital periods and the orbit works as a source of angular momentum for the spin. On the other hand, the Rossby number (the relation between the rotational period and the turnover time of the convective cells, N_R) is strongly related to different activity indicators (Noyes et al. 1984). Then, the relation between Ca II H&K fluxes and Li abundances in CABS is a result of the inhibition of Li depletion caused by high rotation (due to tidal forces present in CABS), while increasing the stellar activity.

There is an alternative explanation for the relation between activity and Li abundance and for the high abundances found in CABS. This explanation relies in the mixing due to internal gravity waves generated by the pressure fluctuation of the convective cells at the bottom of convective envelope on the stellar interior (García López & Spruit 1991; Montalbán 1994). Montalbán (1994) shows how this mechanism produces a macroscopic diffusion, which transports Li (and other elements) toward the internal layers, where it is destroyed. On the other hand, strong magnetic fields in the bottom of the convective envelope, which are responsible of the stellar activity, can inhibit the generation of gravity waves (Schatzman 1993). In a more general way, the presence of a strong magnetic field could also inhibit turbulent mixing mechanisms between the base of the convection zone and the stellar interior (Spruit 1987). This would explain

the link between activity and Li abundance and also the high abundances obtained in CABS. The actual data cannot discriminate which mechanism is actually working. Only a detailed modeling of the evolution of Li abundances and other stellar properties will help to find the answer.

7. Summary and conclusions

We have presented a study of Li abundances in dwarf components of chromospherically active binary stars. The accuracy in the measurements of masses and radii for an important part of the binaries studied here, suggests the use of these data to check different theories about the Li depletion phenomenon.

Since CABS as a group contains binaries in very different evolutionary stages, we first classified the totality of binaries listed in the catalog compiled by Strassmeier et al. (1993). This classification was based on the position of each component in a color-magnitude diagram. We selected stars located in the MS and those beyond the terminal age main sequence, but only if they have not reached the bottom of the red giant branch.

The study of the Li abundances in our sample shows that these stars present abundances higher than the normal values characteristic of stars of the same mass and age. This conclusion was reached by comparing our CABS, whose ages were derived by isochrone-fitting with masses and radii, with open cluster stars. The comparison between stars in the range $1.2-1.4 \text{ M}_{\odot}$ –the cool side of the Li gap– belonging to the M67 and the CABS, of similar ages, shows that Li depletion is not very sensitive to binarity in this mass range. However, notorious overabundances appear for CABS with $0.75 \leq \text{Mass} \leq 0.95 \text{ M}_{\odot}$.

We have also confirmed the presence of a trend between the surface flux in CaII H&K and the Li abundance for CABS in specific mass ranges. We have interpreted this relation and the Li excesses in the context of the transport of angular momentum from the orbit to the spin, due to a tidal effect. This transport produces high rotational rates in these old stars (they do not spin down as single dwarfs do). Because they are, essentially, near the TAMS, they have deep convective envelopes and, hence, low Rossby numbers (a very enhanced activity). On the other hand, the interchange of angular momentum also avoids the radial differential rotation between the convective envelope and the radiative core. Therefore, the turbulent mixing which may appear due to this effect in single stars, leading to Li depletion, would be inhibited and Li would be preserved till certain extent. In short, active stars would have less differential rotation and more Li photospheric abundance than less active stars, explaining the relation between Li and Ca II H&K emission. However, the data do not rule out other explanations such as the transport induced by internal gravity waves and its inhibition due to strong magnetic fields present at the bottom of the convective envelope.

Acknowledgements. This research has made use of the Simbad database, operated at CDS, Strasbourg, France. We greatly appreciate the comments and suggestion on this paper by the referee, R. Gratton. DBN acknowledges the support by the Universidad Complutense with a grant and by the Real Colegio Complutense at Harvard University. This work has been partially supported by the Spanish Dirección General de Investigación Científica y Técnica (DGICYT) under projects PB92-0434-c02-01 and PB94-0203.

References

Andersen, J., Gustafsson, B., and Lambert, D. L., 1984, A&A 136, 65

- Balachandran, S., Lambert, D.L., Sauffer, J.R., 1988, ApJ 333, 267
- Balachandran, S., 1994, in "Cool Stars, Stellar Systems, and the Sun", ed. J.-P. Caillault, APS Conf. Series, vol. 64, p. 234 Balachandran, S., 1995, ApJ 446, 203
- Barrado, D., Fernández-Figueroa, M.J., De Castro, E., Cornide, M., 1993, in "Advances in Stellar and Solar Coronal Physics", eds. Linsky, J. y Serio, S., Kluwer Academic Publishers. p. 299.
- Barrado, D., Fernández-Figueroa, M. J., Montesinos, B., De Castro, E, Cornide, M., 1994, A&A 290, 137 (Paper I)
- Barrado y Navascués, D., 1996, Ph. D. Thesis. Universidad Complutense de Madrid
- Barrado y Navascués, D. and Stauffer, J.R., 1996, A&A 310, 879
- Barrado y Navascués, D., Stauffer, J.R., Hartmann, L., Balachandran, S., 1997a, ApJ 475, 313
- Barrado y Navascués et al. 1997b, in preparation (Paper III)
- Barrado y Navascués et al. 1997c, in preparation
- Boesgaard, A. M., and Tripicco, M.J., 1986a, ApJS 302, L49
- Boesgaard, A.M., and Tripicco, M.J., 1986b, ApJ 303, 724
- Boesgaard, A.M., and Budge, K.G., 1988, ApJ 325, 749
- Boesgaard, A.M., and Budge, K.G., Ramsay M.E., 1988, ApJ 327, 389
- Butler, R.P., Marcy, G.W., Cohen, R.D., Duncan, D.K., 1987, ApJ 319, L19
- Carney, B.W., 1983, AJ 88, 623
- Cayrel, R., Cayrel de Stroebel, G., Campbell, B., Däppen, W., 1984, ApJ 283, 205
- Cayrel, R., Cayrel de Strobel, G., Campbell, B., 1985, A&A 146, 249

- Chaboyer, B.C., 1993, Ph.D. Thesis, Yale University
- Chaboyer, B., Demarque, P., Pinsonneault, M.H., 1995, ApJ 441, 876
- Deliyannis. C.P. and Malaney, R.A., 1995, ApJ 453, 819
- Dempsey, R.C., Linsky, J.L., Fleming, T.A., Schmitt, J.H.M.M., 1993, ApJS 86, 599
- Duncan, D.K. and Jones, B.F., 1983, ApJ 271, 663
- Eker, Z., 1992, ApJS 79, 481
- Favata, F., Micela, G., Sciortino, S., 1996, A&A 311, 951
- Fernández-Figueroa, M. J., Barrado, D., De Castro, E., Cornide, M., 1993, A&A 274, 373
- Fernández-Figueroa, M.J., Montes, D., De Castro, E., Cornide, M., 1994, A&A ApJS 90, 433
- García López, R. J., Rebolo, R., Beckman, J.E., 1988, PASP 100, 1489
- García López, R. J., and Spruit, H. C., 1991, ApJ 377, 268
- García López, R. J., Rebolo, R., Martín, E. L. 1994, A&A 282, 518
- Giampapa, M.S., 1984, ApJ 277, 235
- Gilroy, K., K., 1989, ApJ 347, 835
- Hobbs, L.M. and Pilachowski, C., 1986a, ApJ 308, 854
- Hobbs, L.M. and Pilachowski, C., 1986b, ApJ 311, 37 $\,$
- Hobbs, L. M., and Thorburn, J. A. 1994, ApJ 428, L25
- Houdebine, E.R. and Doyle, J.G., 1995, A&A 302, 861
- Iben, I., 1965, ApJ 142, 1446
- Martín, E.L. and Claret, A., 1996, A&A 306, 408
- Martín, E. L., Rebolo, R., Magazzù, A., and Pavlenko, Ya. V. 1994, A&A 282, 503
- McKeith, C. D., García López, R. J., Rebolo, R., Barnett, E. W., Beckman, J. E., Martín, E. L., and Trapero, J. 1993, A&A 273, 331
- Mermilliod, J.-C., 1981, A&A 93, 136
- Meynet, G., Mermilliod, J.-C., Maeder, A., 1993, A&AS 98, 477
- Montalbán, J. 1994, A&A 281, 421
- Montes, D., Fernández-Figueroa, M.J., De Castro, E., Cornide, M., 1995, A&A 294, 165
- Montes, D., Fernádez-Figueroa, M.J., Cornide, M., De Castro, E., 1996, A&A 312, 221
- Montgomery, K.A., Marschall, L.A., Janes, K.A., 1993, AJ 106, 181
- Noyes, R.W., Hartmann, L.W., Baliunas, S.L., Duncan, D.K., Vaughan, A.H., 1984, ApJ 279, 763
- Pallavicini, R., Cerruti-Sola, M., Duncan, D.K., 1987, A&A 174, 116
- Pallavicini, R., Randich, S., and Giampapa, M. S., 1992, A&A 253, 185
- Pallavicini, R., Cutispoto, G., Randich, S., Gratton, R., 1993, A&A 267, 145
- Pavlenko, Ya. V., Rebolo, R., Martín, E. L., and García López, R. J. 1995, A&A 303, 807
- Pilachowski, C., and Hobbs, L.M., 1987, PASP 99, 1208
- Pinsonneault, M. H., Kawaler, S. D., Sofia, S., Demarque, P., 1989, ApJ 338, 424
- Pinsonneault, M. H., Kawaler, S. D., Demarque, P., 1990, ApJS 74, 501
- Pinsonneault, M. H., Deliyannis, C. P., Demarque, P., 1992, ApJS 78, 179
- Randich. S., Pallavicini, R., 1991, Mem. Soc. Astron. Ital. 62, 75
- Randich. S., Gratton, R., Pallavicini, R., 1993, A&A 273, 194
- Rebolo, R. and Beckman, J.E., 1988, A&A 201, 100
- Ryan, S.G. and Deliyannis, C.P., 1995, ApJ 453, 819
- Schaller, G., Schaerer, D., Meynet, G., Maeder, A., 1992, A&AS 96, 269
- Schaerer, D., Meynet, G., Maeder, A., Schaller, G., 1993a, A&AS 98, 523
- Schaerer, D., Charbonnel, C., Meynet, G., Maeder, A., Schaller, G., 1993b, A&AS 102, 339
- Schatzman, E. 1993, A&A 271, L29
- Schmidt-Kaler, T., 1982 in: Landolt-Börnstein, Vol. 2b, eds. K. Schaifers, H. H. Voig. Springer, Heidelberg
- Smith, V., Lambert, D. L., and Nissen, P. E. 1993, ApJ 408, 262
- Soderblom, D.R., Oey, M.S., Johnson, D.R.H., Stone, R.P.S., 1990, AJ 99, 595
- Soderblom, D.R., Jones, B.F., Balachandran, S., Stauffer, J.R., Duncan, D.K., Fedele, S.B., Hudon, J.D., 1993, AJ 106, 1059
- Spite, F., Spite, M., Peterson, R.C., Chaffee, F.H.Jr., 1987, A& 171, L8
- Spite, M., Pasquini, L., Spite, F., 1994, A&A 290, 217
- Spruit, H. C. 1987, in The Internal Solar Angular Velocity: Theory and Observations, B. R. Durney and S. Sofia (eds.), (Reidel: Dordrecht), p. 185
- Strassmeier, K.G., Hall, D.S., Fekel, F.C., Scheck, M., 1993, A&AS 100, 173
- Thorburn, J.S., Hobbs, L.M., Deliyannis, C.P., Pinsonneault, M.H., 1993, ApJ 415, 150
- VandenBerg, D.H., 1985, ApJS 58, 711
- Zahn, J.-P., 1994, A&A 288, 829

FIGURE CAPTIONS

Figure 1.- Color-magnitude diagram for the totality of CABS listed in Strassmeier et al. (1993). This figure allows the classification of these binaries in five different groups. Symbols for the primary and secondary components are labeled with p and s, respectively.

Figure 2.- Examples of fits to the Li and Fe features.

Figure 3.- Lithium abundance against effective temperature. **a** In this panel, we show our dwarf components of CABS as solid circles, members of Hyades as open circles and stars belonging to Pleiades as open triangles. The average abundance for single Hyades stars is shown as a solid line. **b** Comparison between the abundances of Li of CABS –circles–, the sample of nearby dwarfs by Favata et al. 1995 –crosses for actual data and triangles for upper limits– and the lithium depletion isochrones by Chaboyer (1993) for 50, 70, 300, 600 and 1700 Myr –solid lines.

Figure 4.- Lithium abundance against stellar mass. **a** TLBS CABS are shown as solid triangles, whereas those CABS without the coupling are represented as solid circles. Those Hyades binaries with synchronizarion are shown as open squares. The average Li abundances of Hyades stars are shown as a solid line. This figure eliminates the evolutionary effect on the effective temperature. **b** Comparison with NGC752. **c** Comparison with M67. **d** Comparison with NGC188.

Figure 5.- Li abundance against stellar age. Sizes increase with increasing stellar mass. Fits for single stars belonging to open clusters are shown as solid lines (\sim 1.1, 1.0 and 0.9 M \odot). Error bars are also shown.

Figure 6.- Relation between Li abundances and the surface fluxes in Ca II H&K. Symbol sizes increase with stellar masses.

This article was processed by the author using Springer-Verlag $IAT_{FX} A\&A$ style file L-AA version 3.

 Table 1. Photometry and evolutionary classification of the sample

Name (1) 13 Cet A p 13 Cet A s CF Tuc s CF Tuc p	$\begin{array}{r} \text{HD} \\ (2) \\ \hline 3196 \end{array}$	(U-B) (3)	(B-V) (4)	$(V-R)_j$	$(R-I)_j$	D	V	Mv(d,V)	Lum	$\operatorname{Sp.type}$	Comments
13 Cet A p 13 Cet A s CF Tuc s		(3)		(5)	(6)	(7)	(8)	(9)	(10)	(11)	(12)
13 Cet A s CF Tuc s		0.080	0.570	0.470	0.290	21.3	5.200	3.558	off	{F7V/}	a,kc
CF Tuc s	3196	_	_	_	_	21.3		_	MS	[1 · · /] _	0,110
	5303	0.180	_	_	_	54.0	_	4.4	MS	G0V	c,j
	5303	_	0.735	0.626	0.472	54.0	_	3.748	off	K4IV	a,kc
	14643	0.380	0.850	0.620	0.483	77.0	8.190	3.758	off	G1Vp	a,kc
	17084	0.210	0.730	0.640	0.458		7.990	5.3	MS	G5-8V	a,kc,j
=	17433	0.630	0.960	0.610	0.554	21.0	6.900	5.289	off	K3-4V-IV	a,kc
V471 Tau p	-	0.410	0.900 0.870	0.010 0.750	0.520	59.0	9.710	5.886	MS	K2V	a,d,i
AG Dor p	26354	0.630	0.950	0.794	0.520 0.544		8.670	6.15	MS	K1Vp	a,u,i a,kc,j
EI Eri p	26334 26337	0.030 0.140	0.350 0.670	0.610	0.344 0.390	75.0	6.960	2.585	off	G5IV	а,кс,ј а
	20337 27130	0.140 0.330	0.070 0.775		0.350 0.254	44.7	8.313	5.158	MS	G6V G6V	a,i
	27130 27130	-	-	_	-	44.7	0.010	7.73	MS	K6V	j.
	27691	0.090	0.560	_	0.330		7.000	4.4	MS	G0V	
-		$0.090 \\ 0.335$			0.550				MS	G0V K0V	a,j
	28291		0.746	-		167	8.590	5.9 7.046	MS		a,j
_	283750	0.950	1.085	0.947	0.738	16.7	8.160	7.046		dK5e Vav	a,kc
	283882	0.920	1.060	—	0.420	42.0	10.423	7.307	MS	K3V Kav	b L
	283882	0.920	1.060	-	0.420	42.0	10.423	7.307	MS	K3V Kov	b ·
	30957	—	—	—	—	_	9.353	6.4	MS	K2V K0V	j
	30957	-	-	-	-	-	9.353	6.4	MS	K2V	j
-	31738	0.200	0.710	-	-	60.0	7.120	3.229	off	G5IV	a
YY Gem	-	1.040	1.350	1.340	1.06	13.7	9.823	9.139	MS	dM1e	b
	57853	0.050	0.590	-	-	26.0	6.600	4.525	MS	F9.5V	a
	65626	0.165	0.620	-	_	38.0	6.500	2.5	off	F9IV	a,d,k
	65626	-	-	-	—	38.0	-	2.88	off	G5IV	k , ,
° 1	77137	0.260	0.720	0.550	_	55.0	6.835	3.9	off	G5IV	a,d,e,h
	77137	-	0.760	—	_	55.0	-	3.8	off	G5IV	h
	98230	0.220	0.590	—	_	7.9	4.870	5.382	MS	G5V	a
DF UMa p	-	—	0.890	—	_	22.7	10.140	8.389	MS	dM0e	a,i
DF UMa s	-	-	_	—	_	22.7	-	12.3	MS	[dM5]	j
	101309	_	_	-	_	62.0	_	5.1	MS	G5V	j
	108102	-0.010	0.510	0.400	0.300	86.0	8.833	4.161	MS	F8V	b
	108102	-0.010	0.510	0.400	0.300	86.0	8.833	4.161	MS	F8V	b
	114519	0.090	0.420	—	_	180.0	-	2.6	off	F4IV	$^{\rm c,h}$
	143313	0.630	0.940	—	—	30.0	_	6.215	MS	K2V	$_{\rm d,e,i}$
	143313	1.150	1.230	-	-	30.0	-	7.725	MS	K6V	j
	146361	0.000	0.470	0.500	-	21.0	5.700	4.089	MS	F6V	a
	146361	-	-	-	-	21.0	-	4.4	MS	G0V	j
	150708	0.040	0.600	-	-	180.0	-	2.304	off	G2IV	$^{ m d,m}$
	155638	-	0.450	-	-	310.0	-	2.349	off	F2IV	m
	163930	-	0.590	-	-	100.0	7.230	2.9	off	F4V-IV	g,h
	163930	—	-	-	—	100.0	_	3.5	off	K0IV	h
	165590	0.130	0.590	-	—	41.7	-	4.4	MS	G0V	$_{\rm d,e,h}$
	165590	—	_	-	—	41.7	-	5.1	MS	G5V	h
-	165590	1.130	1.360	—	—	41.7	11.373	8.272	MS	K7V	b
	165590	1.130	1.360	-	-	41.7	11.373	8.272	MS	K7V	b
	166181	0.130	0.720	0.540	-	31.0	7.660	5.222	MS	G5V	a,i
	166181	-	-	-	-	31.0	-	9.6	MS	[M1-2V]	j
BY Dra p 2	234677	1.000	1.221	1.100	0.780	15.6	8.070	7.4	MS	K4V	a,d,h
BY Dra s 2	234677	_	_	-	—	15.6	-	8.6	MS	K7.5V	h
V478 Lyr p 1	178450	0.210	0.740	0.650	0.430	26.0	7.680	5.605	MS	G8V	a
HR 7578 1 1	188088	0.940	1.050	0.830	0.480	15.0	6.913	6.753	MS	K2-3V	b
HR 7578 2 1	188088	0.940	1.050	0.830	0.480	15.0	6.913	6.753	MS	K2-3V	b
V1396 Cyg p	-	1.080	1.517	-	0.910	15.9	10.130	9.280	MS	M2V	a,d,i
V1396 Cyg s	-	-	-	-	_	15.9	-	11.3	MS	M4Ve	j

Table 1. Continuation. Photometry and evolutionary classification of the sample

Name	HD	(U-B)	(B-V)	$(V-R)_j$	$(R-I)_j$	D	V	Mv(d,V)	Lum	Sp.type	Comments
(1)	(2)	(3)	(4)	(5)	(6)	(7)	(8)	(9)	(10)	(11)	(12)
ER Vul p	200391	—	0.680	—	—	46.0	7.270	4.62	MS	G0V	a,d,h
ER Vul s	200391	—	—	—	—	46.0	_	4.74	MS	G5V	h
$42 \operatorname{Cap} p$	206301	0.200	0.650	—	0.240	34.0	5.170	2.513	off	G2IV	a
KZ And p	218738	0.550	0.893	_	_	—	8.733	6.4	MS	dK2	b,j
KZ And s	218738	0.550	0.893	—	—	—	8.733	6.4	MS	dK2	b,j
SZ Psc s	219113	0.000	0.440	—	—	125.0	_	3.3	MS	F8IV	h
KT Peg p	222317	0.160	0.670	_	_	22.5	7.040	5.394	MS	G5V	a,l,m
KT Peg s	222317	—	_	_	_	22.5	_	7.820	MS	K6V	l,m

Spectral type between brackets are asumed from the photometry. a.- The color indices include the contribution of the secondary, except when the color for the secondary is given. b.- Two equal stars: $(U-B)_p=(U-B)_s=(U-B)_{obs}$, $V_p=V_s=V_{obs}+0.753$. c.- The hot component dominates (U-B). d.- There is also available M_V^p , M_V^s . e.- It is possible to deconvolve the photometry in V. f.-Combined M_V . g.- The hot component dominates (B-V). h.- $M_V(hot/cool)$ were calculated independently during the eclipses. i.- $M_V(\text{primary})$ were calculated by a deconvolution with the $M_V(\text{total})$ and $M_V(\text{secondary})$: $V_p = V_s - 2.5 \text{ Log } [10^{-(V_{\text{total}} - V_s)/2.5} - 1]$. j.- M_V assumed from the spectral type. k.- From the Strassmeier et al. catalogue. I.- Distance from M_V , V. m.- M_V from R, T_{eff} , CB.

Table 2. Equivalent widths and corrections for the observed stars (in mÅ).

Name	HD	Teff	Radius	EW(Li+Fe)	EW(Fe)	EW(Li)	CCF(c/h)	Comments
		(K)	$({ m R}_{\odot})$	(mÅ)	(mÅ)	(mÅ)		
(1)	(2)	(3)	(4)	(5)	(6)	(7)	(8)	(9)
13 Cet A	3196	6023	_	89	4^{calc}	85^{calc}	_	
VY Ari	17433	4831	-	62	23^{calc}	39^{calc}	_	
EI Eri	26337	5555	_	67	11	55	—	
$BD+64\ 487$	30957	4900	_	54	16	38	2.000	3
$BD+64\ 487$	30957	4900	—	13.5	3	13	2.000	3
V1198 Ori	31738	5517	-	13	3	11	—	
V1198 Ori	31738	-	-	_	-	-	_	
YY Gem	_	3185	-	43	7^{calc}	36^{calc}	2.000	3
YY Gem	_	3185	-	_	-	-	2.000	3
ξ UMa B	98230	5948	-	44	1	33	—	
DF UMa	_	5117	-	68	14^{calc}	52^{calc}	1.027	3
DF UMa	_	3240	—	27	16^{calc}	11^{calc}	37.678	3
MS Ser	143313	4989	_	46	40^{calc}	7^{calc}	1.249	3
MS Ser	143313	4275	—	—	_	-	5.018	3
$\sigma^2 \text{ CrB}$	146361	6444	1.22	30*	4^{calc}	18^{calc}	1.777	1
$\sigma^2 \text{ CrB}$	146361	6030	1.21	60*	7^{calc}	30^{calc}	2.287	1
WW Dra	150708	5910	2.12	87	4	34	2.158	1
WW Dra	150708	4580	3.9	21	13	7	1.863	1,4
V772 Her	165590	5948	1.0	—	_	105^{calc}	1.328	1
V772 Her	165590	5770	0.6	—	-	83^{calc}	4.114	1
ADS 11060C	165590	3979	-	43	33^{calc}	10^{calc}	2.000	3
ADS 11060C	165590	3979	_	—	_	_	2.000	3
V815 Her	166181	5496	0.97	202	10^{calc}	192^{calc}	1.040	1
V815 Her	166181	3648	0.525	—	_	_	26.113	1
V1396 Cyg	_	3752	0.4	52	40	12	1.383	1
V1396 Cyg	_	3370	0.3426	—	-	—	3.611	1
KZ And	218738	5117	—	29	7^{calc}	27^{calc}	2.000	3
KZ And	218738	5117	-	34	7^{calc}	36^{calc}	2.000	3
KT Peg	222317	5528	0.93	17	12	4	1.168	1
KT Peg	222317	4178	0.72	—	_	_	6.937	1

Line blended with others. ¹ CCF from Equation 2 and 3. ² CCF from Equation 2 and 4. ³ We deconvolved the magnitude of the primary from the total magnitude and an estimation of the magnitude of the secondary by using the spectral type. ⁴ Evolved components.

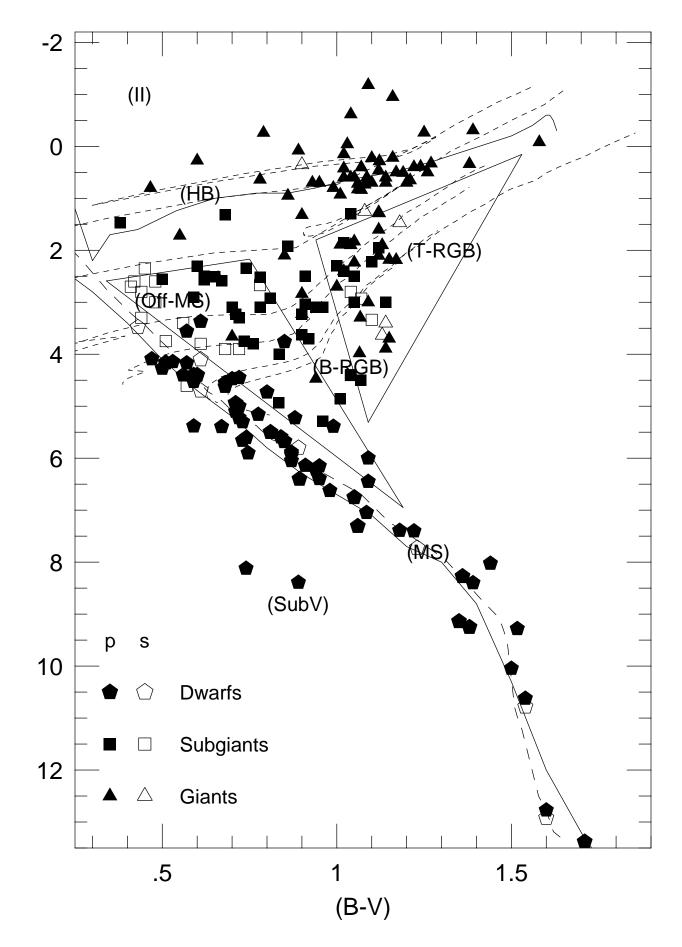
Table 3. Final abundances, where Log $N({\rm Li}){=}12{+}{\rm Log}\{N({\rm Li})/N({\rm H})\},$ and other parameters for CABS

						_	-	
Name	HD	T _{eff}	EWcor	N(Li)	Mass	Porb	P_{phot}	Log Age
		(K)	(mÅ)		(M_{\odot})	(d)	(d)	(yr)
(1)	(2)	(3)	(4)	(5)	(6)	(7)	(8)	(9)
13 Cet A p	3196	6023	85	2.84	$\sim 1.60^{\rm CM}$	2.08200	$\sim 2.08^{\text{Porb}}$	9.221 ^M
13 Cet A s	3196	5700	≤ 1	≤ 0.0	—	2.08200	$\sim 2.08^{\rm Porb}$	$\sim 9.22^{\rm P}$
CF Tuc s	5303	6030	61.29	2.59	1.057	2.79786	2.798	9.892
CF Tuc p	5303	5097	73.49	1.87	1.205	2.79786	2.798	9.812
BQ Hyi p	14643	5140	26.64	1.27	$\sim 1.32^{\rm CM}$	18.379	18.24	$\sim 9.454^{\rm M}$
UX For p	17084	5357	24.49	1.45	—	0.95479	0.957	=
VY Ari p	17433	4831	39	1.10	$\sim 0.80^{\rm CM}$	13.198	16.42	$\sim 10.059^{\mathrm{M}}$
V471 Tau p	-	4752	218.7	2.72	0.8	0.52119299	0.5197	Hyades
AG Dor p	26354	4964	16.46	0.82	≤ 0.80	2.562	2.533	-
EI Eri p	26337	5555	25.65	1.67	_	1.947227	1.945	_
vB22 p	27130	5542	67.3	2.28	1.086	5.609198	$\sim 5.61^{\mathrm{Porb}}$	Hyades
vB22 s	27130	4366	-	—	0.776	5.609198	$\sim 5.61^{ m Porb}$	Hyades
vB40A p	27691	6225	122.3	3.46	—	4.00000	$\sim 4.00^{\rm Porb}$	Hyades
vB 69 p	28291	5539	11.8	1.28	$\sim 0.96^{\rm CM}$	41.66	_	Hyades
V833 Tau p	283750	4540	16.2	0.23	0.8	1.787797	1.797	Hyades
vB117 p	283882	4650	≤ 4.2	≤ -0.25	$\sim 0.79^{{\rm M}{\rm sin}^3{\rm i}}$	11.9293	6.82	Hyades
vB117 s	283882	4520	≤ 2.6	<u>≤</u> -0.65	$\sim 0.77^{\mathrm{Msin^{3}i}}$	11.9293	6.82	Hyades
BD+64 487 1	30957	4900	≤ 2.0 76	≤ -0.03 1.64	/≈ 0.11 ≤0.80	44.38	0.82	ityades
$BD+64 \ 487 \ 2$ $BD+64 \ 487 \ 2$	30957 30957	4900 4900	$\frac{70}{27}$	0.98	$\leq 0.80 \\ < 0.80$	44.38	_	_
V1198 Ori p	31738	$\frac{4900}{5517}$	11	1.23	$\sim 1.84^{\rm CM}$	44.30	-4.55	$\sim 9.059^{\mathrm{M}}$
HR 2814 p	5175853	5917 5948	$11 \\ 101.54$	2.93	~ 1.64	$^{-}$ 122.169	4.55	~ 9.059
YY Gem		3185	65	2.93 0.11	-0.62	0.8142822	- 0.8143	—
	65696	$5185 \\ 5829$	65.70					$\sim 9.194^{\rm M}$
54 Cam p	65626			2.47	1.64	11.06803	10.163	
54 Cam s	65626	5460 5420	116.57	2.71	1.61	11.06803	10.163	$\sim 9.217^{\rm M}$
TY Pyx p	77137	5438	4.53	0.75	1.22	3.198548	3.32	9.730
TY Pyx s	77137	5390 5049	7.05	0.89	1.20	3.198548	$\begin{array}{l} 3.32 \\ \sim 3.98^{\mathrm{Porb}} \end{array}$	9.796
ξ UMa B p	98230	5948	33	2.14	-	3.9805	~ 3.98 $\sim 1.03^{\mathrm{Porb}}$	—
DF UMa p	-	5117	53	1.60	0.56	1.033824	$\sim 1.03^{\circ}$ $\sim 1.00^{ m Porb}$	_
DF UMa s	-	3240	-	-	0.3	1.033824		—
CD-38 7259 s	101309	5770	41.54	2.13	_ 	11.710	11.66	-
IL Com p	108102	6266	22	2.25	0.85	0.9616	0.82	10.054
IL Com s	108102	6266	28	2.37	0.82	0.9616	0.82	10.121
RS CVn s	114519	6700	_	~ 3	1.41	4.797851	4.7912	9.410
MS Ser p	143313	4989	9	0.57	_	9.01490	9.60	—
MS Ser s	143313	4275	-	-	-	9.01490	9.60	-
$\sigma^2 \operatorname{CrB} s$	146361	6444	30	2.61	1.12	1.139791	1.1687	9.611
$\sigma^2 \operatorname{CrB} p$	146361	6030	69	2.67	1.14	1.139791	1.1687	9.648
WW Dra s	150708	5910	48	2.37	1.36	4.629617	4.63	9.575
V792 Her s	155638	6539	81	2.4	1.41	27.5368	27.07	9.422
Z Her p	163930	5948	-	—	1.61	3.992801	3.962	9.012
Z Her s	163930	5000	_	-	1.31	3.992801	3.962	9.675
V772 Her Aa	165590	5948	158	3.19	1.04	0.879504	0.878	9.465
V772 Her B	165590	5770	243	3.60	0.88	7391.25	_	9.465
ADS 11060C p $$	165590	3979	16	-0.43	$\sim 0.70^{{\rm M}{\rm sin}^3{\rm i}}$	25.762	_	V772 Her
ADS 11060C s	165590	3979	_	_	$\sim 0.67^{\rm Msin^3i}$	25.762	_	V772 Her
V815 Her p	166181	5496	201	3.63	$\sim 0.86^{ m RT}$	1.809837	1.819	$\sim 9.972^{\rm M}$
V815 Her s	166181	3648	_	_	_	1.809837	1.819	$\sim 9.972^{\rm P}$
BY Dra p	234677	4300	7	-0.42	~ 0.55	5.975112	3.827	—
BY Dra s	234677	4021	8	-0.65	0.44	5.975112	3.827	—
V478 Lyr p	178450	5395	59	1.97	$\sim 0.83^{\mathrm{RT}}$	2.130514	2.13	$\sim 10.014^{\rm M}$
HR 7578 1	188088	4839	4.91	0.1	≥0.80	46.815	16.5	≤ 9.966
HR 7578 2	188088	4839	4.91	0.1	≥ 0.80	46.815	16.5	≤ 9.966
V1396 Cyg p	- 100000	3752	17	-0.60	$\frac{\geq 0.00}{0.42}$	3.276188	$\sim 3.28^{\text{Porb}}$	_0.000
V1396 Cyg p V1396 Cyg s	_	3370	_	0.00	0.42	3.276188 3.276188	$\sim 3.28^{\mathrm{Porb}}$	_
1 1000 Uyg S		0010			0.41	0.210100	0.20	

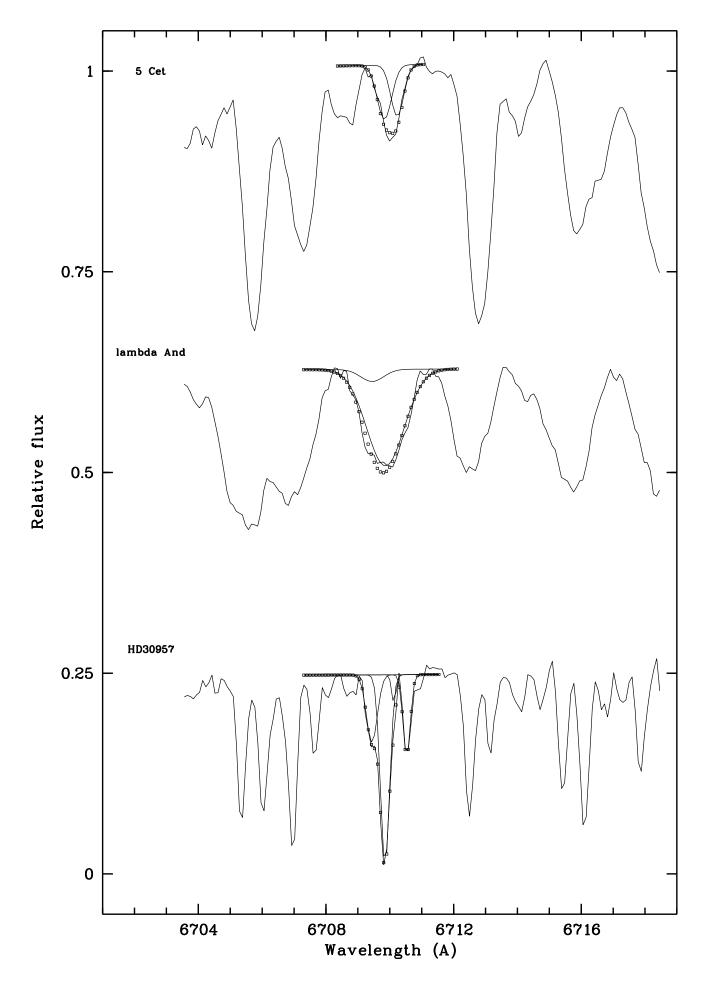
 $\textbf{Table 3. Continuation. Final abundances, where Log N(Li) = 12 + Log \{N(Li)/N(H)\}, and other parameters for CABS N(Li) = 12 + Log \{N(Li)/N(H)\}, and other parameters for CABS N(Li) = 12 + Log \{N(Li)/N(H)\}, and other parameters for CABS N(Li) = 12 + Log \{N(Li)/N(H)\}, and other parameters for CABS N(Li) = 12 + Log \{N(Li)/N(H)\}, and other parameters for CABS N(Li) = 12 + Log \{N(Li)/N(H)\}, and other parameters for CABS N(Li) = 12 + Log \{N(Li)/N(H)\}, and other parameters for CABS N(Li) = 12 + Log \{N(Li)/N(H)\}, and other parameters for CABS N(Li) = 12 + Log \{N(Li)/N(H)\}, and other parameters for CABS N(Li) = 12 + Log \{N(Li)/N(H)\}, and other parameters for CABS N(Li) = 12 + Log \{N(Li)/N(H)\}, and other parameters for CABS N(Li) = 12 + Log \{N(Li)/N(H)\}, and other parameters for CABS N(Li) = 12 + Log \{N(Li)/N(H)\}, and other parameters for CABS N(Li) = 12 + Log \{N(Li)/N(H)\}, and other parameters for CABS N(Li) = 12 + Log \{N(Li)/N(H)\}, and other parameters for CABS N(Li) = 12 + Log \{N(Li)/N(H)\}, and other parameters for CABS N(Li) = 12 + Log \{N(Li)/N(H)\}, and other parameters for CABS N(Li) = 12 + Log \{N(Li)/N(H)\}, and other parameters for CABS N(Li) = 12 + Log \{N(Li)/N(H)\}, and other parameters for CABS N(Li) = 12 + Log \{N(Li)/N(H)\}, and other parameters for CABS N(Li) = 12 + Log \{N(Li)/N(H)\}, and other parameters for CABS N(Li) = 12 + Log \{N(Li)/N(H)\}, and other parameters for CABS N(Li) = 12 + Log \{N(Li)/N(H)\}, and other parameters for CABS N(Li) = 12 + Log \{N(Li)/N(H)\}, and other parameters for CABS N(Li) = 12 + Log \{N(Li)/N(H)\}, and other parameters for CABS N(Li) = 12 + Log \{N(Li)/N(H)\}, and other parameters for CABS N(Li) = 12 + Log \{N(Li)/N(H)\}, and other parameters for CABS N(Li) = 12 + Log \{N(Li)/N(H)\}, and other parameters for CABS N(Li) = 12 + Log \{N(Li)/N(H)\}, and other parameters for CABS N(Li) = 12 + Log \{N(Li)/N(H)\}, and other parameters for CABS N(Li) = 12 + Log \{N(Li)/N(H)\}, and other parameters for CABS N(Li) = 12 + Log \{N(Li)/N(H)\}, and other parameters for CABS N(Li) = 12 + Log \{N(Li)/N(H)\}, and othe$

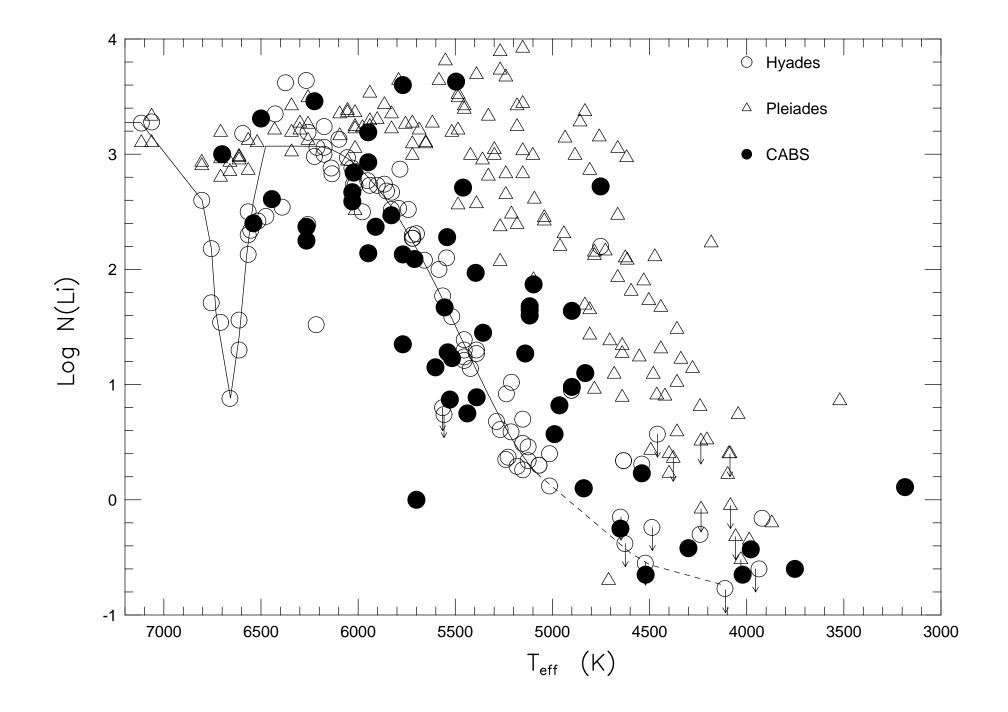
Name	HD	$T_{\rm eff}$	EW_{cor}	N(Li)	Mass	$\mathbf{P}_{\mathrm{orb}}$	$P_{\rm phot}$	Log Age
		(K)	(mÅ)		(M_{\odot})	(d)	(d)	(yr)
(1)	(2)	(3)	(4)	(5)	(6)	(7)	(8)	(9)
ER Vul p	200391	5602	≤ 8	≤ 1.15	1.10	0.6980951	0.6942	9.569
ER Vul s	200391	5770	≤ 9	≤ 1.35	1.05	0.6980951	0.6942	9.748
$42 \operatorname{Cap} p$	206301	5710	42.07	2.09	$\sim 2.58^{\rm CM}$	13.1740	$\sim 13.17^{\rm Porb}$	$\sim 8.649^{\mathrm{M}}$
KZ And p	218738	5117	58	1.65	$\sim 0.66^{\mathrm{Msin}^{3}\mathrm{i}}$	13.1740	3.03	_
KZ And s	218738	5117	62	1.68	0.63	3.032867	3.03	—
SZ Psc s	219113	6500	75.50	3.31	1.28	3.032867	3.955	9.496
KT Peg p	222317	5528	4	0.87	0.93	6.201986	6.092	9.926
KT Peg s	222317	5528	-	_	0.62	6.201986	6.092	$\sim 9.926^{\rm P}$

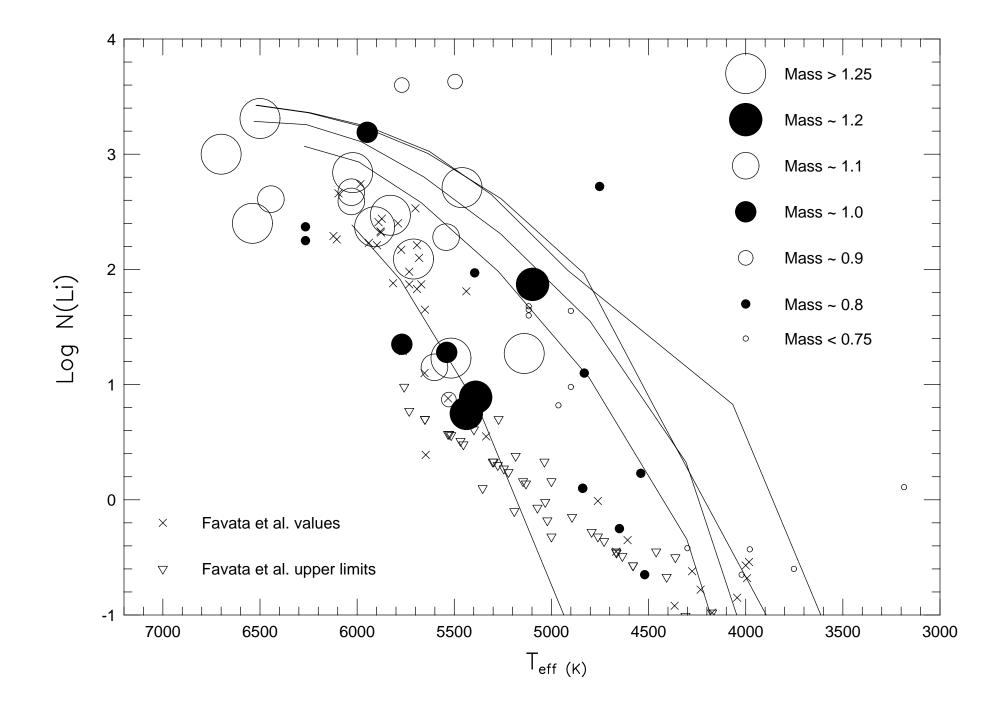
CM.- Mass estimated from the color-magnitud diagram. Porb.- Photometric preiod similar to the orbital value. M.- Age estimated from the mass-age realtionship. P.- Age of the secondary equal to the computed age for the primary. Msin³i.- Mass computed from $M \times sin^3$ i. RT.- Mass estimated from Radii- T_{eff} plane.

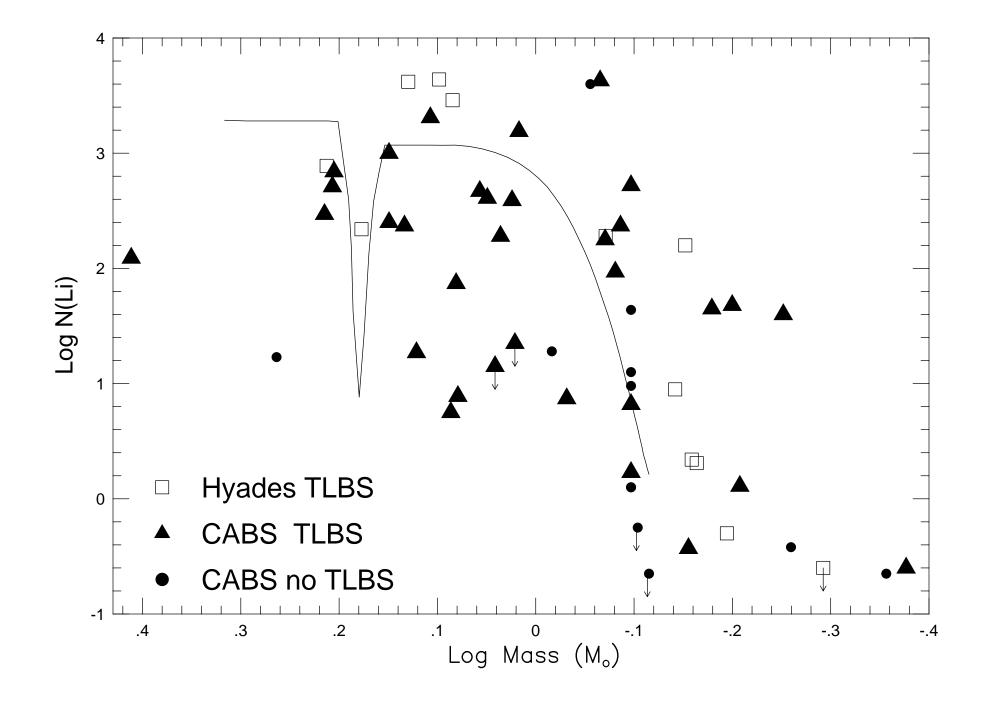


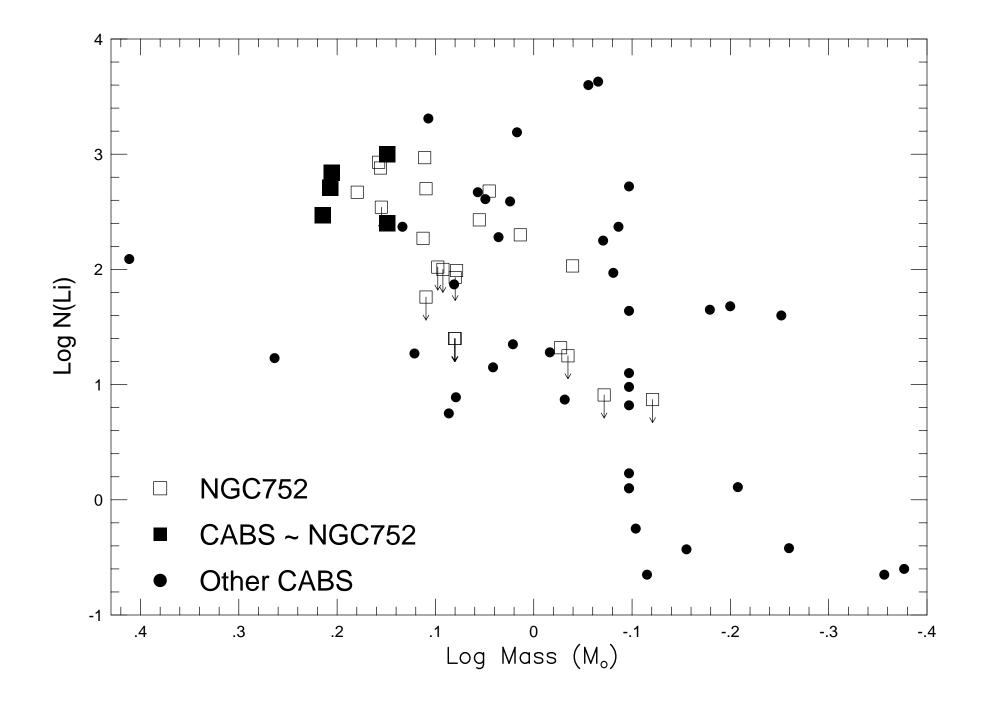
Ž

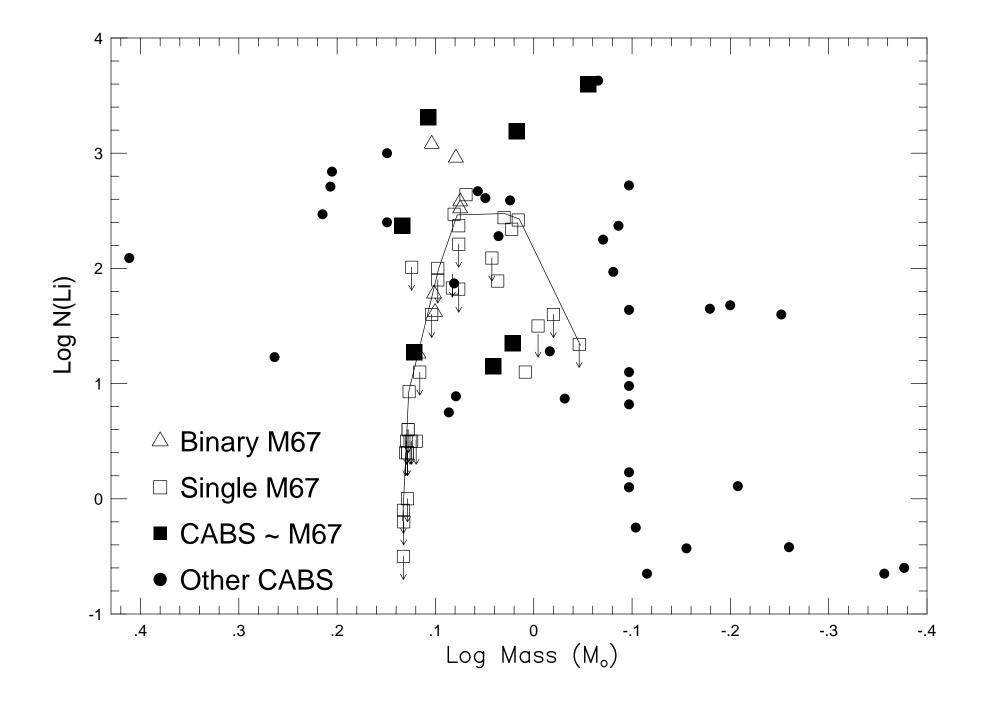


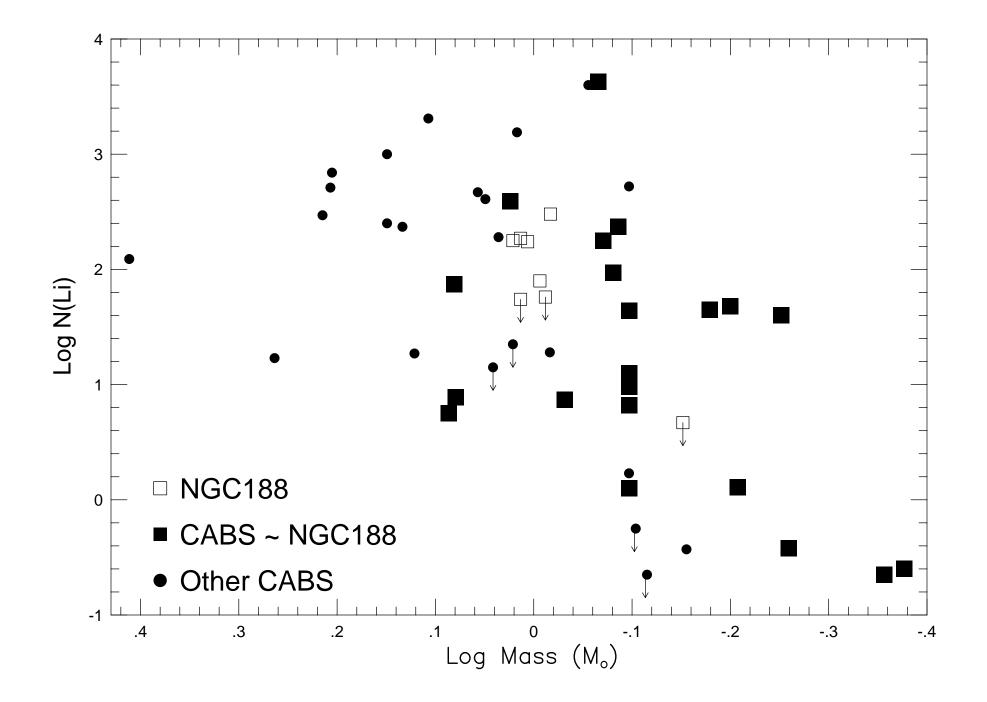


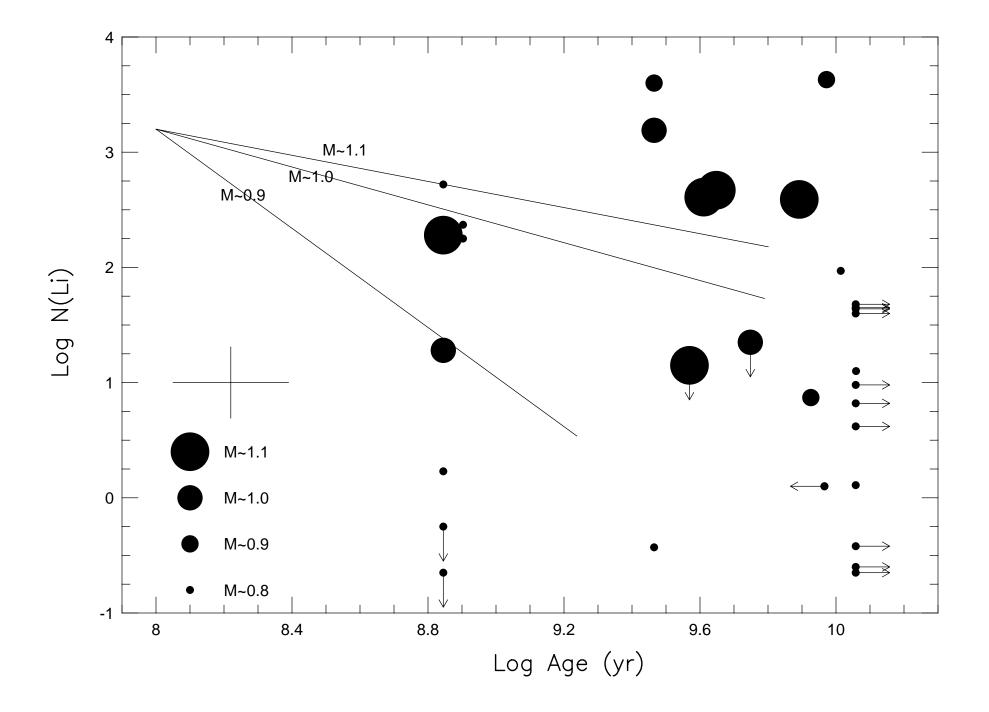




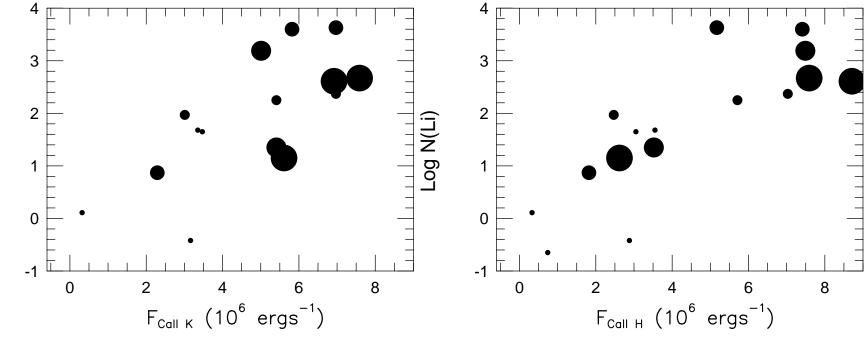












Log N(Li)